

Length-Dependent Enantioselectivity of Carbon Nanotubes by Gel Chromatography

Xiaojun Wei,* Xin Luo, Shilong Li, Weiya Zhou, Sishen Xie, and Huaping Liu*



Cite This: <https://doi.org/10.1021/acsnano.2c12853>



Read Online

ACCESS |



Metrics & More



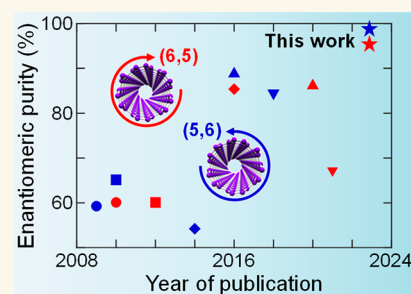
Article Recommendations



Supporting Information

ABSTRACT: High-purity enantiomer separation of chiral single-wall carbon nanotubes (SWCNTs) remains a challenge compared with electrical type and chirality separations due to the limited selectivities for both chirality and handedness, which is important for an exploration of their properties and practical applications. Here, we performed length fractionation for enantiomer-purified SWCNTs and found a phenomenon in which the enantioselectivities were higher for longer nanotubes than for shorter nanotubes due to length-dependent interactions with the gel medium, which provided an effective strategy of controlling nanotube length for high-purity enantiomer separation. Furthermore, we employed a gentler pulsed ultrasonication instead of traditional vigorous ultrasonication for preparation of a low-defect long SWCNT dispersion and achieved the enantiomer separation of single-chirality (6,5) SWCNTs with an ultrahigh enantiomeric purity of up to 98%, which was determined by using the linear relationship between the normalized circular dichroism intensity and the enantiomeric purity. Compared with all results reported previously, the present enantiomeric purity was significantly higher and reached the highest level reported to date. Due to the ultrahigh selectivity in both chirality and handedness, the two obtained enantiomers exhibited perfect symmetry in their circular dichroism spectra, which offers standardization for characterizations and evaluations of SWCNT enantiomers.

KEYWORDS: single-wall carbon nanotubes, enantiomer separation, enantiomeric purity, length fractionation, single-chirality, pulsed ultrasonication, gel chromatography



1. INTRODUCTION

Single-wall carbon nanotubes (SWCNTs) can be divided into armchair, zigzag, and chiral species according to their chiral angles.¹ As the most abundant species, chiral SWCNTs contain a pair of enantiomers with different handedness.² The enantiomers of single-chirality SWCNTs have important applications in the high-precision detection and purification of chiral molecules, including proteins, DNA, and drug molecules,^{3–8} due to their highly selective interactions with chiral molecules derived from the single helix structure. For example, Pu et al. developed an electrochemical sensor enabling chiral differentiation of L-DOPA and D-DOPA by employing enantiomers of single-chirality (6,5) SWCNTs to create a chiral space on a glassy-carbon electrode.⁵ In addition, the enantiomers of single-chirality (6,5) SWCNTs were also used to create near-infrared (NIR) fluorescent sensors for several important analytes, such as L-ascorbic acid, D-isoascorbic acid, L-adrenaline, and D-adrenaline.⁶ However, the selectivities of these chiral molecules are generally limited by the enantiomeric purity (EP) of the single-chirality SWCNTs, which constitutes a serious problem in practical applications. Therefore, the production of high-purity single-chirality enantiomers is still highly desired, which is of great significance not only for practical applications but also for the

explorations of their unknown properties. The high-purity single-chirality enantiomers will also enable us to probe and unlock the complex chiral behaviors of various biochemical systems due to their single-molecule recognition and detection capabilities.⁹

Because a selective synthesis of either enantiomer has not been successful to date, postsynthetic enantiomer separation is the only way to control the handedness of SWCNTs.⁷ To achieve this goal, various separation methods, including molecular recognition,^{10–12} density gradient ultracentrifugation (DGU),^{13,14} DNA-based aqueous two-phase extraction (ATP),^{15,16} and gel chromatography,^{17–19} have been developed. Actually, these methods are being developed and continuously improved from metallic/semiconducting to single-chirality and to enantiomer separation. Compared with well-studied metallic/semiconducting and single-chirality separations, single-chirality enantiomer separation is the ultimate

Received: December 29, 2022

Accepted: April 21, 2023

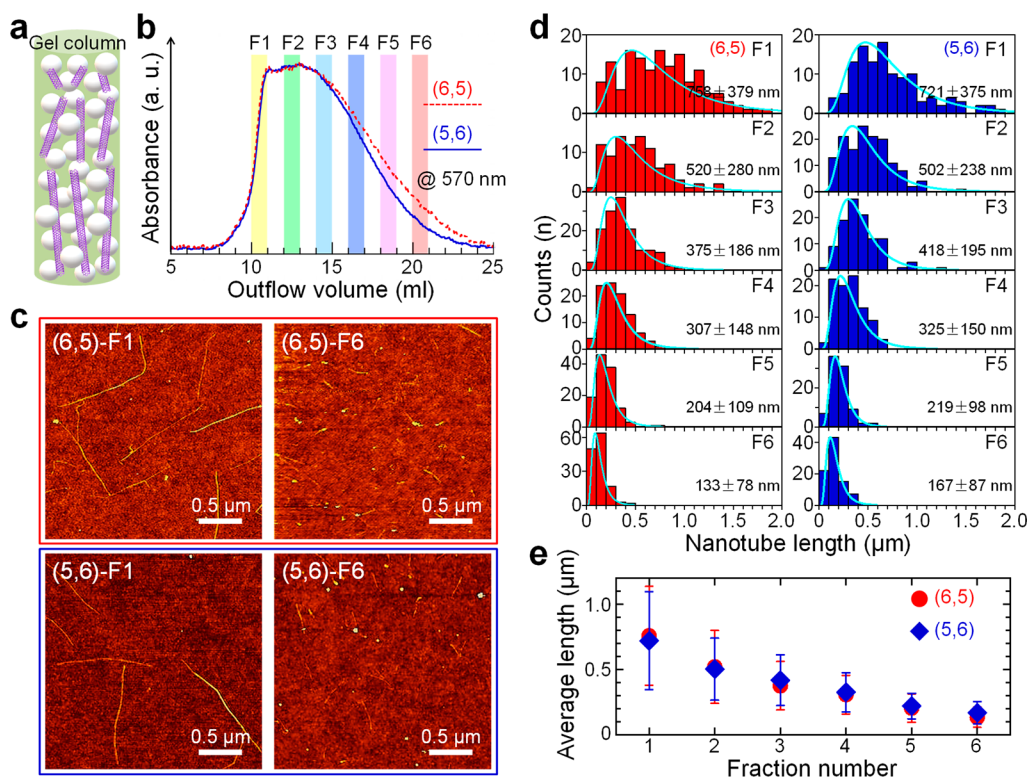


Figure 1. (a) Schematic diagram for length fractionation of SWCNTs using a long gel column. (b) UV chromatograms of the outflow solutions at 570 nm for (6,5) and (5,6) SWCNTs prepared from CoMoCAT material. (c, d) Typical AFM images and corresponding length distributions of F1 and F6 fractions for (6,5) and (5,6) SWCNTs. (e) Plot of the average length of fractionated (6,5) and (5,6) SWCNTs as a function of fraction number. The results for (6,5) and (5,6) SWCNTs are indicated in red and blue, respectively.

structure separation of SWCNTs and is usually more difficult because it requires more precise techniques to achieve chirality and handedness selectivity. Therefore, high-purity enantiomer separation of single-chirality SWCNTs remains a challenge. Recently, an evaluation method of EP based on the linear relationship between the circular dichroism (CD) intensity normalized by absorbance and EP was established,²⁰ which made us realize the insufficient EPs of obtained SWCNT enantiomers. Through this evaluation method, we found that the EPs of (6,5) SWCNTs separated by molecular recognition and DGU methods were less than 70%,^{10,11,13,14,21} while the higher EPs of SWCNTs separated by gel chromatography and ATP methods were still less than 90%.^{15,17,19,22,23} Therefore, compared with the separation purities of metallic/semiconducting and single-chirality SWCNTs,^{16,24–33} there is still much room for improvement in the EPs of single-chirality SWCNTs.

To further improve the EPs of single-chirality SWCNTs, we must take into account the characteristics of the chiral SWCNTs themselves, in addition to potential improvements in the separation technique. It is well-known that dispersing pristine SWCNTs in solutions of various dispersants (such as surfactants, DNA, and polymers) with the assistance of ultrasonication is generally required before separation,³⁴ which inevitably introduces defects into the nanotubes and shortens the nanotube lengths. Although the reduction in nanotube lengths does not in principle affect the electronic structures of the two enantiomers,³⁵ it may affect the interactions between dispersant molecules and the two enantiomers and thus reduce the inherent enantioselectivity of a specific separation method. Despite this, details on the

effect of length on separation of SWCNT enantiomers have not been reported to date.

In this work, we systematically investigated the influence of length on the enantioselectivity of gel chromatography by using enantiomer-purified (6,5) SWCNTs with different length distributions. As a result, the CD intensities were found to be higher for long nanotubes than for short nanotubes. After excluding the possibility of intrinsic length-dependent CD spectral strength, the CD intensity variations were confirmed to originate from the differences in enantioselectivity of SWCNTs with different lengths during separation. Based on this finding, a strategy of controlling nanotube length was proposed for high-purity enantiomer separation. Furthermore, we employed a gentler pulsed ultrasonication instead of traditional vigorous ultrasonication to reduce the shortening effect during the dispersion of pristine SWCNTs. Using the prepared low-defect long SWCNT dispersion, enantiomers of single-chirality (6,5) SWCNTs with ultrahigh purities of up to 98% were successfully separated via mixed-surfactant gel chromatography. Compared with the highest EP reported previously, 89%, the present EP was higher and exceeded the common level of chirality separation. The obtained high-purity single-chirality enantiomers are more beneficial for research on fundamental properties and applications of chiral SWCNTs.

2. RESULTS AND DISCUSSION

We prepared the enantiomer-purified (6,5) and (5,6) SWCNTs from CoMoCAT material by using stepwise elution chromatography, as reported previously (the details are described in the [Experimental Section](#)),²² and then performed their length fractionation with size exclusion chromatogra-

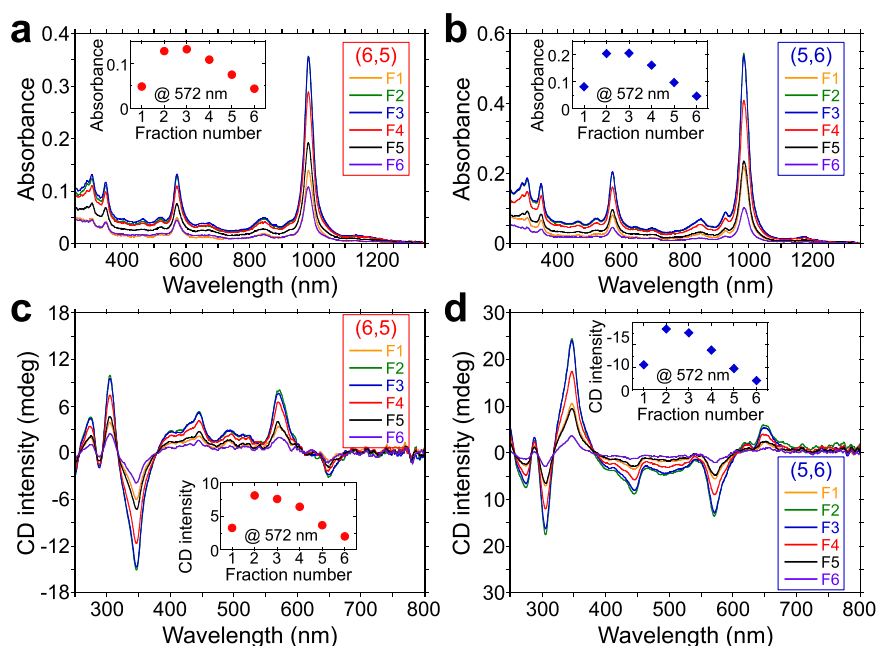


Figure 2. (a, b) Optical absorption spectra for fractions F1–F6 for (6,5) (a) and (5,6) (b) SWCNTs. Insets: plots of E_{22} absorbance at 572 nm for each fraction. (c, d) CD spectra of F1–F6 fractions for (6,5) (c) and (5,6) (d) SWCNTs. Insets: plots of E_{22} CD intensities at 572 nm for each fraction.

phy.^{36–39} To obtain a good fractionation effect, a long column (Tricorn 10/300, GE Healthcare) filled with ~24 mL of gel (Sephacryl S-1000, GE Healthcare) was used. After loading ~1 mL of a high-concentration (6,5) or (5,6) SWCNT solution into the equilibrated gel column, 1% sodium cholate (SC) aqueous solution was injected into the column to wash out the SWCNTs with different lengths. Every 1 mL of outflow solution from the column was sequentially recovered using a fraction collector. Because the SWCNTs were dispersed in 1% SC solution that is usually used to elute the SWCNTs adsorbed on a gel column, there was no structural selectivity for chirality or enantiomers, except for nanotube sizes (Figure 1a). Figure 1b shows the UV chromatogram detected at 570 nm (close to the E_{22} transition wavelength of (6,5) and (5,6) SWCNTs) for the outflow solution. The UV chromatogram clearly shows that the SWCNTs were mainly contained in the 9th–22nd mL of outflow solution. Therefore, 6 fractions (denoted as F1–F6) were selected for the following morphological and spectral characterizations.

Figure 1c shows typical atomic force microscopy (AFM) images for the F1 and F6 fractions of the (6,5) and (5,6) SWCNTs. The AFM images for other fractions are shown in Figure S1. It can be clearly observed that the earlier outflow F1 solution contained much longer nanotubes than the later outflow F6 solution. This outflow order for nanotube length is consistent with previous results.^{36–40} We systematically counted the length distribution of each fraction (more than 100 nanotubes) for (6,5) and (5,6) SWCNTs (Figure 1d). As a result, a monotonic reduction in the average length was observed as the fraction number increased, as shown in Figure 1e. The average lengths were estimated to be 758 ± 379 and 721 ± 375 nm for the F1 fractions of the (6,5) and (5,6) SWCNTs, respectively, which were reduced to 133 ± 78 and 167 ± 87 nm for the F6 fractions of the (6,5) and (5,6) SWCNTs, indicating good fractionation of the length with the present size exclusion chromatography. The length distribu-

tions of (6,5) and (5,6) SWCNTs before length fractionation are shown in Figure S2. Since there was no significant difference in average length and the difference between the length-fractionated (6,5) and (5,6) SWCNTs, the initial shortening effect and current fractionation effect were considered to be the same for (6,5) and (5,6) SWCNTs.

Figure 2a,b shows the optical absorption spectra for each fraction of the (6,5) and (5,6) SWCNTs. The E_{22} absorbance at 572 nm for each fraction is plotted in the inset to demonstrate their concentration changes. Although the nanotube concentrations of each fraction were different, their E_{11} or E_{22} transition wavelengths were the same (Figure S3). However, when each absorption spectrum was normalized by its E_{11} absorbance, we found that the E_{22} absorbance increased with increasing fraction number (Figure S4). This likely occurred because the amorphous carbon contents of the later fractions were higher than those of the earlier fractions.^{41–43} This explanation is reasonable because the particle sizes of amorphous carbon are closer to those of the short nanotubes contained in the later fractions. A similar E_{22} absorbance increase with increasing fraction number was also observed for length-fractionated pristine CoMoCAT SWCNTs. The corresponding Raman spectral measurement demonstrated that the intensity ratio of G^+ to defect band decreased with increasing fraction number (Figure S5). The Raman spectra of length-fractionated (6,5) or (5,6) SWCNTs were not measured due to the limitation of laser wavelength corresponding to the E_{22} transition of SWCNTs.

Figure 2c,d shows the CD spectra for each fraction of the (6,5) and (5,6) SWCNTs, which were measured with a CD spectropolarimeter. The E_{22} CD intensities at 572 nm for each fraction are also plotted in the insets. As with the change in E_{22} absorbance values plotted in the insets of Figure 2a,b, the E_{22} CD intensity first increased and then decreased with increasing fraction number, suggesting that the CD intensity changes were mainly contributed by the differences in nanotube

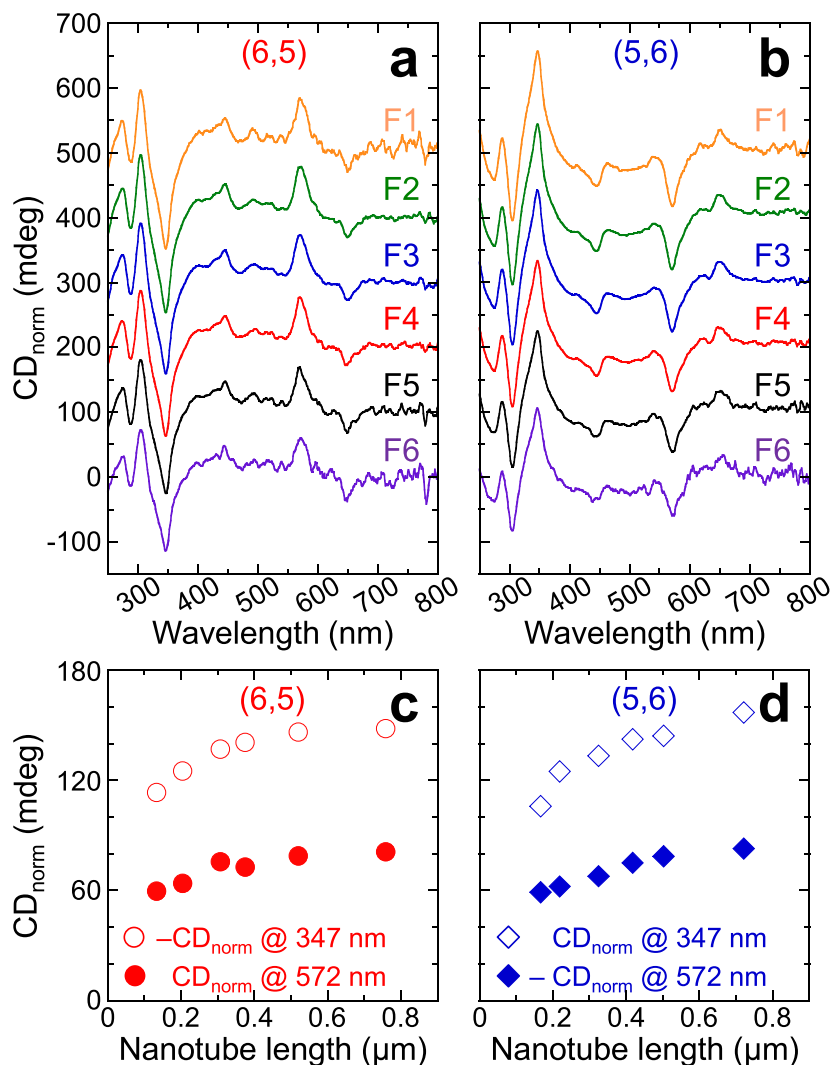


Figure 3. (a, b) CD spectra of F1–F6 fractions for (6,5) (a) and (5,6) (b) SWCNTs. Each spectrum was normalized by the calibrated E_{22} absorbance and vertically shifted for comparisons of CD_{norm} intensities. (c, d) Plot of CD_{norm} (or $-CD_{\text{norm}}$) intensities at 572 nm (solid symbols) and 347 nm (open symbols) for fractionated (6,5) (c) and (5,6) (d) SWCNTs as a function of nanotube length.

concentrations. Despite this, we still noticed a small detail; the highest E_{22} CD intensities appeared in the F2 fractions for both (6,5) and (5,6) SWCNTs, which was slightly inconsistent with the E_{22} absorbances. Although the s/n ratios of several fractions were limited due to their low nanotube concentrations, the CD spectral sharpness was confirmed to be the same for all fractions through spectral normalization (Figure S6). This differed from the optical absorption spectra, indicating that amorphous carbon only contributed to the optical absorption, not to the CD signal. Therefore, the absorption for amorphous carbon should be removed to obtain a true E_{22} absorbance and CD_{norm} value. If not, the EP determined from the CD_{norm} value will be underestimated.

Figure 3a,b shows the CD spectra normalized by the E_{22} absorbance for fractions F1–F6 of the (6,5) and (5,6) SWCNTs, where the E_{22} absorbance values used were calibrated by subtracting the background absorption of amorphous carbon (Figures S7 and S8). To observe the changes in the CD_{norm} values more clearly, we plotted the CD_{norm} values at the E_{22} transition wavelength (572 nm), accompanied by those at the E_{33} transition wavelength (347 nm) with higher s/n ratios, as a function of nanotube length

(Figure 3c,d). As a result, the absolute value of CD_{norm} at the E_{22} (E_{33}) transition wavelength was found to gradually increase from 59.6 mdeg (113.4 mdeg) to 81.2 mdeg (148.1 mdeg) for the (6,5) SWCNTs and from 59.0 mdeg (105.8 mdeg) to 82.8 mdeg (156.9 mdeg) for the (5,6) SWCNTs. This large change in the CD_{norm} value was undoubtedly not caused only by the low s/n ratios of CD spectra or background removal of absorption spectra. In contrast, for the (6,5) and (5,6) SWCNTs before length fractionation, the absolute values of CD_{norm} at the E_{22} (E_{33}) transition wavelength were 73.7 mdeg (138.8 mdeg) for the (6,5) SWCNTs and 76.4 mdeg (144.2 mdeg) for the (5,6) SWCNTs. These values were at intermediate levels, compared with those of fractions F1–F6 (Figure S9).

Before exploring the reason for the decrease in the CD_{norm} value, we first considered the possibility of intrinsic length-dependent CD intensity for the SWCNT enantiomers. Previous studies have investigated the length dependence of SWCNT optical responses, including absorption, photoluminescence, and Raman scattering.^{44–49} However, the length dependence of CD intensity of SWCNT enantiomers has not been investigated. Therefore, we performed a controlled

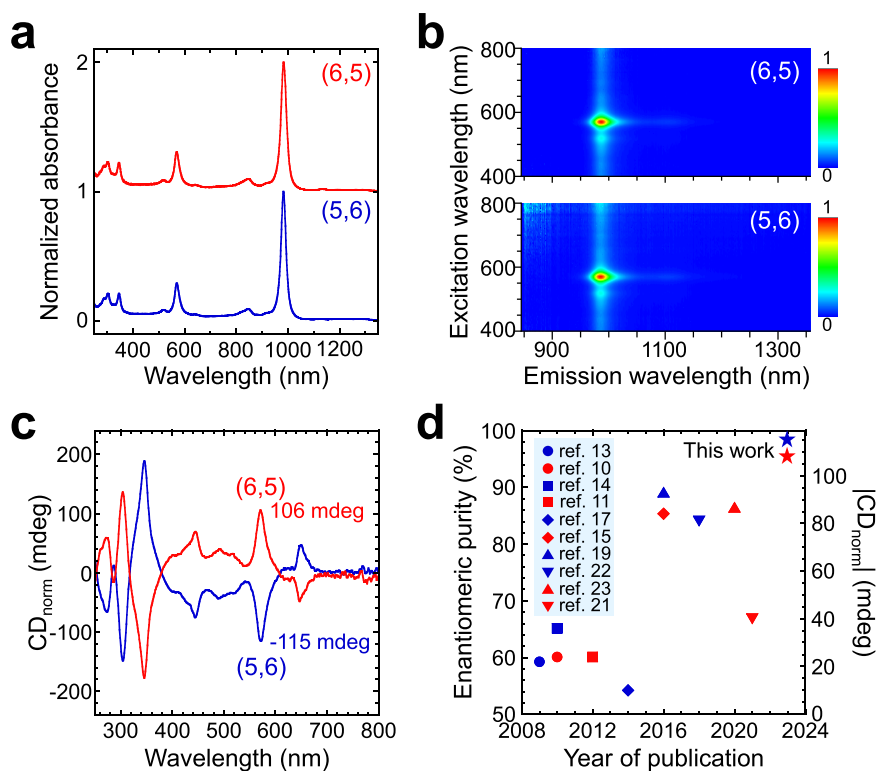


Figure 4. (a–c) Optical absorption spectra (a), photoluminescence contour maps (b), and CD spectra (c) of (6,5) and (5,6) SWCNTs separated from the HiPco SWCNT dispersion prepared by pulsed ultrasonication for 1 h. (d) Comparison of the EPs for (6,5) (red symbols) or (5,6) (blue symbols) SWCNTs separated by different separation methods, accompanied by the corresponding absolute values of CD_{norm} .

experiment to shorten the nanotube lengths of enantiomer-purified SWCNTs by using ultrasonication treatments for various times. After confirming the reduction in nanotube length and the increase in relative emission intensity derived from oxygen doping with increasing ultrasonication time, we found that both the optical absorbance and CD intensity decreased slightly, while the CD_{norm} value did not change (Figure S10). The decrease in optical absorbance was in agreement with length-dependent optical effects reported previously.⁴⁶ The decrease in CD intensity was also understandable because the CD intensity is proportional to the differences in absorbance between left and right circularly polarized light for chiral substances. The simultaneous decrease in both optical absorbance and CD intensity resulted in a constant CD_{norm} value. Therefore, the possibility of CD_{norm} dependence on the length can basically be excluded.

Another explanation for the fraction-dependent CD_{norm} value shown in Figure 3 is that the earlier fraction containing longer nanotubes had a higher EP than the later fraction. Because there was no chirality or enantiomer selectivity during length fractionation, different enantioselectivities should result during prior enantiomer separation of single-chirality SWCNTs. It is well-known that enantiomer separations of SWCNTs are strongly dependent on chiral dispersants due to their different interactions with the two enantiomers.^{7,15,20} When the SWCNTs are inevitably shortened during vigorous ultrasonication dispersion, the handedness periodicity of a SWCNT decreases with decreasing nanotube length. If the interaction difference per handedness periodicity between two enantiomers is fixed, the shortening effect will dramatically reduce the overall difference in the interactions of two enantiomers with the dispersant molecules, limiting the

inherent enantioselectivity of the gel chromatography method. Back to the enantiomer separation based on stepwise elution chromatography (Experimental Section), coating the sodium deoxycholate (DOC) surfactants to (5,6) and then to (6,5) enantiomers resulted in their separation, but the difference of the change in the amount of coated DOC surfactants between (5,6) and (6,5) should be larger for longer nanotubes than for shorter nanotubes (Figure S11). The larger difference in DOC coating means a higher enantiomeric resolution. Therefore, the longer SWCNTs exhibited higher enantioselectivities than the shorter SWCNTs. The experimental verification will be performed elsewhere. Despite this, this explanation originates from the change of surfactant coating required for structure separation of SWCNTs, which is well consistent with present separation results and is in principle consistent with the mechanism of surfactant-based enantiomer separation by an ATP method reported recently.⁵⁰ In addition to length, we should also consider a defect effect that may also have affected the enantioselectivity of SWCNTs because the defect density is in principle higher for shorter SWCNTs than for longer SWCNTs. The introduction of defects, including vacancy and covalent forms,⁵¹ will break the perfect symmetry of a pair of enantiomers, which is the basis for enantioselectivity. In gel chromatography based enantiomer separation, symmetry breaking means that the difference in the interactions between chiral surfactants and two enantiomers should be reduced. At the same time, the difference in the affinities between the optically active dextran-based gel and two enantiomers should also be reduced. This leads to lower enantioselectivity for high-defect nanotubes than for low-defect nanotubes. Moreover, this defect- or length-induced reduction in the enantioselectivities of SWCNTs is likely to occur in other liquid separation

methods because of their similar enantiomer separation mechanisms. If our speculation is true, controlling the lengths and defects of SWCNTs would be an effective way to achieve high-purity enantiomer separation.

It should be mentioned that, as described above, the (6,5) and (5,6) SWCNTs used for examining the length-dependent enantioselectivity were prepared from CoMoCAT material because CoMoCAT makes it easier to prepare high-concentration (6,5) and (5,6) SWCNT solutions for length fractionation due to their high contents. In contrast, another SWCNT material produced by high-pressure catalytic CO decomposition (HiPco) was mainly used to prepare a low-defect long SWCNT dispersion for the following enantiomer separation of single-chirality SWCNTs because the HiPco has a more obvious advantage in separation purity compared with CoMoCAT. Detailed separation results of HiPco and CoMoCAT materials and their comparison will be described below. To prepare a low-defect long HiPco or CoMoCAT SWCNT dispersion, we developed a gentler pulsed ultrasonication method (the details are described in the [Experimental Section](#)). Compared with traditional vigorous ultrasonication widely used, pulsed ultrasonication effectively avoided a continuous shock of high-frequency vibration from the ultrasonication tip, reducing the damage to the inherent carbon hexagonal structures of SWCNTs. Simultaneously, good dispersion of the SWCNTs can be verified by confirming the results of subsequent chirality and enantiomer separation. After dispersion, a portion of the short SWCNTs was further removed by the length fractionation described above. After obtaining the long-SWCNT dispersion, we also prepared the short-SWCNT dispersion by nonpulsed continuous ultrasonication for 10 h for comparison. [Figure S12](#) shows the typical AFM images and corresponding length distributions of the resulting long and short SWCNTs. Their average lengths were estimated to be 479 ± 253 and 222 ± 97 nm, respectively. The Raman spectral measurements further demonstrated the difference in the intensity ratio of G^+ to the defect band in the Raman spectrum (~ 105 for the long SWCNTs and ~ 60 for the short SWCNTs, [Figure S13](#)), suggesting their different defect contents.^{52,53} Using these two SWCNT dispersions, the method of mixed-surfactant gel chromatography we reported previously was employed for enantiomer separation of single-chirality SWCNTs.^{19,54} The detailed separation procedures are described in the [Experimental Section](#).

[Figure 4a](#) shows the optical absorption spectra of the (6,5) and (5,6) SWCNTs separated from the long-SWCNT dispersion. Both spectra exhibited a series of sharp absorption peaks corresponding to E_{ii} transitions. In addition, two weak peaks corresponding to phonon sidebands of the E_{11} and E_{22} transitions can be clearly observed at 846 and 518 nm for both the (6,5) and (5,6) SWCNTs. No other chirality species can be identified from these two absorption spectra and the corresponding photoluminescence contour maps ([Figure 4b](#)), indicating high chirality purity. The optical chirality purity was basically higher than 99% (see [Figure S14](#) for an evaluation of the chirality purity based on a common peak fitting method for the experimental optical absorption spectrum), which exceeded the spectral detection accuracy. The ultrahigh chirality purity should have resulted from the high enrichment of chirality species for adsorbed SWCNTs on the gel and high chirality resolution during stepwise elution ([Figure S15](#)). Furthermore, both spectra exhibited very low background

absorption, especially in the NIR range, indicating that most impurities, including amorphous carbon and nanotube bundles, were effectively removed during separation. This should have been contributed by pH control of the gel chromatography, as described in the [Experimental Section](#).²⁸ Such high chirality purity and low background absorption mean that the experimentally measured absorbance was almost entirely derived from the (6,5) and (5,6) SWCNTs. Therefore, the values for the E_{22} absorbance can be used directly to calculate CD_{norm} , avoiding possible errors resulting from the complex decomposition procedures of different chirality species and background absorption. [Figure 4c](#) shows the CD spectra of the separated (6,5) and (5,6) SWCNTs, in which the CD intensity was normalized by the E_{22} absorbance. The CD_{norm} values at the E_{22} transition wavelength were estimated to be 106 and -115 mdeg for the (6,5) and (5,6) SWCNTs, respectively. Both CD_{norm} values were much higher than previous results, including the highest values we have reported (85 mdeg for the (6,5) and -93 mdeg for the (5,6) SWCNTs).¹⁹ Furthermore, due to ultrahigh selectivities for both chirality and handedness, the two separated enantiomers exhibited perfect symmetry in their CD spectra ([Figure S16](#)), which offers promise for use as a standard in characterizations and evaluations of SWCNT enantiomers.

Compared with the previous dispersions produced by nonpulsed continuous ultrasonication for 20 h,¹⁹ the SWCNT dispersion used in this work was prepared by using the gentler pulsed ultrasonication for only 1 h. Because we adopted the same method of mixed-surfactant gel chromatography for separation of the (6,5) and (5,6) SWCNTs, the enantioselectivities of the separation methods should be approximately the same. Therefore, the improved enantioselectivity (CD_{norm} value) should be attributed to the much gentler shortening effect of the dispersion process. To further verify the length-dependent enantioselectivity, a controlled separation experiment using the short-SWCNT dispersion was also performed by applying the same separation procedure. As a result, the CD_{norm} values of the separated (6,5) and (5,6) SWCNTs decreased to 87 and -102 mdeg, respectively.

Based on the linear relationship reported previously for the EP and the CD_{norm} intensity,²⁰ the EPs of the obtained (6,5) and (5,6) SWCNTs can be estimated to be 95% and 98%, respectively. We noticed that the EP of the (6,5) SWCNTs was lower than that of the (5,6) SWCNTs due to imperfect enantiomeric resolution by the adopted mixed surfactant. In other words, the (5,6) SWCNTs adsorbed on the gel were not completely eluted in the early elution step, and thus, small amounts of residual (5,6) SWCNTs were inevitably eluted along with the (6,5) SWCNTs in the later elution step. On the other hand, compared with the CoMoCAT material ([Figure 3](#)), the present (6,5) and (5,6) SWCNTs separated from HiPco showed higher EPs, suggesting that the enantiomeric selectivity is dependent not only on the nanotube length but also on the growth method of pristine SWCNT material. To compare the separation purities of HiPco and CoMoCAT materials, we also prepared the low-defect long CoMoCAT SWCNT dispersion using the same dispersion and length fractionation conditions, and then performed the enantiomer separation of single-chirality SWCNTs using the same separation procedures as described in the [Experimental Section](#). As shown in [Figure S17](#), similar to HiPco, only a few chirality species, (6,4), (6,5), and (7,5) were adsorbed on the gel for CoMoCAT, and their elution orders were also

strongly dependent on nanotube diameter. However, the chirality purities and EPs of separated (6,5) and (5,6) SWCNTs are lower for CoMoCAT than for HiPco (Figure S18), in which (6,4) SWCNTs are always present as an impurity for CoMoCAT and may affect the E_{22} absorbance and CD_{norm} values of separated (6,5) or (5,6) SWCNTs due to their similar E_{22} transition wavelengths. This should be attributed to the higher (6,4) content for pristine CoMoCAT than for pristine HiPco that leads to more (6,4) SWCNTs adsorbed on the gel (Figure S19). Unlike the raw HiPco without any additional treatment, the CoMoCAT SWCNTs utilized here were treated after growth, which may make CoMoCAT SWCNTs harder to disperse and thus affect their chirality and enantiomeric selectivity. Although HiPco SWCNTs were previously used for the separation of single-chirality SWCNTs,^{17,19} such a high enantiomeric selectivity has not been achieved. In contrast, length shortening was deliberately avoided by reducing the impact of ultrasonication in this work, which is an important reason for the improvement in enantiomeric selectivity. As shown in Figure 4d, the absolute values of CD_{norm} and the corresponding EPs for the (6,5) or (5,6) SWCNTs separated by different separation methods were plotted for comparison. It is clear that the present EP was significantly higher, and it reached the highest level reported to date. More importantly, unlike the traditional iterative separation method used to improve the target purity,^{27,32} the high EP was achieved with only one round of enantiomer separation, indicating that gel chromatography is the most efficient method for separation of SWCNT enantiomers thus far.

3. CONCLUSION

In summary, we performed length fractionation with enantiomer-purified SWCNTs and found a phenomenon in which the enantioselectivity was higher for long nanotubes than for short nanotubes. Based on this finding, we revealed an effective strategy of controlling nanotube length for high-purity enantiomer separation. Using the low-defect long SWCNT dispersion prepared with the gentler pulsed ultrasonication method, the enantiomers of single-chirality (6,5) SWCNTs with ultrahigh EPs of up to 98% were successfully separated by mixed-surfactant gel chromatography. The present EP was significantly higher than those reported previously, and it reached a near-perfect level. We believe that this work will facilitate the emergence of more unforeseeable properties and applications of SWCNT enantiomers in the near future.

4. EXPERIMENTAL SECTION

4.1. Preparation of (6,5) and (5,6) Enantiomers for Length Fractionation. First, the CoMoCAT SWCNTs (Sigma-Aldrich) dispersed in 0.5% SC (purity $\geq 99.0\%$, Sigma-Aldrich) + 0.5% sodium dodecyl sulfate (SDS, purity $\geq 99.0\%$, Sigma-Aldrich) solution were directly injected into a gel column (Sephacryl S-200, GE Healthcare) equilibrated with a 0.5% SC + 0.5% SDS solution. After collecting the unadsorbed SWCNTs by washing with the 0.5% SC + 0.5% SDS solution, we performed the stepwise elution for the adsorbed SWCNTs using 0.5% SC + 0.5% SDS + $x\%$ DOC (purity $\geq 97.0\%$, Sigma-Aldrich) solutions, in which the DOC concentration (x) was increased stepwise from 0 to 0.06%. Finally, the enantiomer-purified (5,6) and (6,5) SWCNTs were obtained at DOC concentrations of 0.028 and 0.031, respectively (CD spectra are shown in Figure S9). More details are described in our previous report.²²

4.2. Preparation of Low-Defect Long SWCNT Dispersions Using Pulsed Ultrasonication. SWCNTs produced by high-

pressure catalytic CO decomposition (HiPco, Raw, Nopo Nanotechnologies India Private Limited) were used as the starting material without additional treatment. Forty milligrams of the SWCNT powder was dispersed in 40 mL of a 1% SC aqueous solution using a 1 s on/off pulsed ultrasonic homogenizer (output 30%, Sonifier 450D, Branson) for 1 or 10 h (on-state time) at 20 °C. After ultrasonication, the solution was ultracentrifuged for 1 h in an angle rotor (S50A, 210000g, Hitachi Koki) to remove catalytic metal particles, nanotube bundles, and impurities. The upper 80% of the supernatant was recovered as a pristine SWCNT dispersion. For comparison, the low-defect long CoMoCAT SWCNT dispersion was also prepared by using the same ultrasonication and ultracentrifugation conditions. Before separation, SDS was added to the pristine SWCNT dispersion to create a mixed surfactant system comprising 0.5% SC + 1.5% SDS.

4.3. Separation of (6,5) and (5,6) SWCNT Enantiomers Using Mixed-Surfactant Gel Chromatography. The HiPco SWCNTs dispersed in 0.5% SC + 1.5% SDS solution were injected into a syringe column packed with ~ 80 mL of gel (Sephacryl S-200, GE Healthcare) equilibrated with the 0.5% SC + 1.5% SDS solution at 24 °C. The unadsorbed fraction containing the (6,5), (5,6), and other large-chiral-angle SWCNTs was collected, followed by washing with the same solution, while the small-chiral-angle SWCNTs were adsorbed onto the gel column. Subsequently, the same amount of 0.5% SC solution was added to the unadsorbed SWCNT solution to create a mixed surfactant comprising 0.5% SC + 0.75% SDS for adsorption of the (6,5) and (5,6) SWCNTs on the gel. To reduce the adsorption of amorphous carbon on the gel, the pH of the unadsorbed SWCNT solution was adjusted to ~ 8.4 with formic acid (purity $\geq 95\%$, Sigma-Aldrich). After injecting the unadsorbed SWCNT solution into a cleaned gel column (~ 30 mL) and then washing with the 0.5% SC + 0.75% SDS solution, the environment of the gel column was gradually changed to 0.5% SC + 0.5% SDS for the following enantiomer separation. As we reported previously, aqueous solutions of 0.5% SC + 0.5% SDS + $x\%$ DOC were used for stepwise elution of the SWCNTs adsorbed on the gel column, and the DOC concentration (x) was increased stepwise. Finally, the SWCNTs eluted at DOC concentrations of 0.028 and 0.031 were confirmed to be (5,6) and (6,5), respectively, by measuring their optical absorption and CD spectra, as shown in Figure 4. To compare the separation results of HiPco and CoMoCAT materials, the CoMoCAT SWCNT dispersion prepared above was also used for separation of (6,5) and (5,6) SWCNT enantiomers by using the same separation conditions.

4.4. Optical Measurements. Optical absorption spectra were measured from 1400 to 200 nm using an ultraviolet–visible near-infrared spectrophotometer (UV-3600, Shimadzu). Photoluminescence spectra were measured using a spectrofluorometer (Nanolog, HORIBA) equipped with a liquid-nitrogen-cooled InGaAs NIR array detector. A 450 W xenon lamp was used for sample excitation. All raw intensities were corrected for the intensities of the lamp spectrum. CD spectra were measured from 800 to 200 nm in 1 nm increments using a CD spectropolarimeter (J-1500, JASCO). Raman spectra were measured using a high-resolution confocal micro-Raman spectrometer (HRS-500SS, Princeton Instruments) equipped with a liquid-nitrogen-cooled charge-coupled device detector (PYL-100BRX, Princeton Instruments). A laser with a wavelength of 633 nm was selected to excite the SWCNTs.

ASSOCIATED CONTENT

Supporting Information

The Supporting Information is available free of charge at <https://pubs.acs.org/doi/10.1021/acsnano.2c12853>.

Details for the AFM images of (6,5) and (5,6) SWCNTs before and after length fractionation, comparison of optical absorption, CD, and Raman spectra for length-fractionated SWCNTs, subtraction of background absorption, schematic diagram of length-dependent enantioselectivity, comparison of long and short SWCNTs, peak fitting of the experimental absorption

spectra, and optical absorption spectra of SWCNTs eluted at different DOC concentrations, and comparison of separation results of HiPco and CoMoCAT SWCNTs (PDF)

AUTHOR INFORMATION

Corresponding Authors

Xiaojun Wei – Beijing National Laboratory for Condensed Matter Physics, Institute of Physics, Chinese Academy of Sciences, Beijing 100190, People's Republic of China; Department of Physics and Center of Materials Science and Optoelectronics Engineering, University of Chinese Academy of Sciences, Beijing 100049, People's Republic of China; Beijing Key Laboratory for Advanced Functional Materials and Structure Research, Beijing 100190, People's Republic of China; Songshan Lake Materials Laboratory, Dongguan, Guangdong 523808, People's Republic of China; orcid.org/0000-0002-8746-6641; Email: weixiaojun@iphy.ac.cn

Huaping Liu – Beijing National Laboratory for Condensed Matter Physics, Institute of Physics, Chinese Academy of Sciences, Beijing 100190, People's Republic of China; Department of Physics and Center of Materials Science and Optoelectronics Engineering, University of Chinese Academy of Sciences, Beijing 100049, People's Republic of China; Beijing Key Laboratory for Advanced Functional Materials and Structure Research, Beijing 100190, People's Republic of China; Songshan Lake Materials Laboratory, Dongguan, Guangdong 523808, People's Republic of China; orcid.org/0000-0001-7017-4127; Email: liuhuaping@iphy.ac.cn

Authors

Xin Luo – Beijing National Laboratory for Condensed Matter Physics, Institute of Physics, Chinese Academy of Sciences, Beijing 100190, People's Republic of China; Department of Optoelectronic, Xiamen University of Technology, Xiamen, Fujian 361024, People's Republic of China

Shilong Li – Beijing National Laboratory for Condensed Matter Physics, Institute of Physics, Chinese Academy of Sciences, Beijing 100190, People's Republic of China; Beijing Key Laboratory for Advanced Functional Materials and Structure Research, Beijing 100190, People's Republic of China; orcid.org/0000-0002-6355-7143

Weiya Zhou – Beijing National Laboratory for Condensed Matter Physics, Institute of Physics, Chinese Academy of Sciences, Beijing 100190, People's Republic of China; Department of Physics and Center of Materials Science and Optoelectronics Engineering, University of Chinese Academy of Sciences, Beijing 100049, People's Republic of China; Beijing Key Laboratory for Advanced Functional Materials and Structure Research, Beijing 100190, People's Republic of China; Songshan Lake Materials Laboratory, Dongguan, Guangdong 523808, People's Republic of China; orcid.org/0000-0001-6851-1630

Sishen Xie – Beijing National Laboratory for Condensed Matter Physics, Institute of Physics, Chinese Academy of Sciences, Beijing 100190, People's Republic of China; Department of Physics and Center of Materials Science and Optoelectronics Engineering, University of Chinese Academy of Sciences, Beijing 100049, People's Republic of China; Beijing Key Laboratory for Advanced Functional Materials and Structure Research, Beijing 100190, People's Republic of

China; Songshan Lake Materials Laboratory, Dongguan, Guangdong 523808, People's Republic of China

Complete contact information is available at:
<https://pubs.acs.org/10.1021/acsnano.2c12853>

Notes

The authors declare no competing financial interest.

ACKNOWLEDGMENTS

We thank Prof. Hiromichi Kataura (National Institute of Advanced Industrial Science and Technology, AIST) and Prof. Riichiro Saito (Tohoku University) for helpful discussions on the optical effect of SWCNTs with different lengths and defects. This work was supported by the National Key Research and Development Program of China (grant nos. 2020YFA0714700 and 2018YFA0208402), the National Natural Science Foundation of China (grant nos. 51820105002, 11634014, 51872320, and 52172060), the Strategic Priority Research Program of the Chinese Academy of Sciences (grant no. XDB33030100), the Key Research Program of Frontier Sciences, CAS (grant no. QYZDBSSW-SYS028), and the Youth Innovation Promotion Association of CAS (grant no. 2020005).

REFERENCES

- (1) Wilder, J. W. G.; Venema, L. C.; Rinzler, A. G.; Smalley, R. E.; Dekker, C. Electronic structure of atomically resolved carbon nanotubes. *Nature* **1998**, *391*, 59–62.
- (2) Samsonidze, G. G.; Grüneis, A.; Saito, R.; Jorio, A.; Souza Filho, A. G.; Dresselhaus, G.; Dresselhaus, M. S. Interband optical transitions in left- and right-handed single-wall carbon nanotubes. *Phys. Rev. B* **2004**, *69*, 205402.
- (3) Power, T. D.; Skoulidas, A. I.; Sholl, D. S. Can chiral single walled carbon nanotubes be used as enantiospecific adsorbents? *J. Am. Chem. Soc.* **2002**, *124*, 1858–1859.
- (4) Yoo, J.; Ozawa, H.; Fujigaya, T.; Nakashima, N. Evaluation of affinity of molecules for carbon nanotubes. *Nanoscale* **2011**, *3*, 2517–2522.
- (5) Pu, C.; Xu, Y.; Liu, Q.; Zhu, A.; Shi, G. Enantiomers of single chirality nanotube as chiral recognition interface for enhanced electrochemical chiral analysis. *Anal. Chem.* **2019**, *91*, 3015–3020.
- (6) Nißler, R.; Kurth, L.; Li, H.; Spreinat, A.; Kuhlemann, I.; Flavel, B. S.; Kruss, S. Sensing with chirality-pure near-infrared fluorescent carbon nanotubes. *Anal. Chem.* **2021**, *93*, 6446–6455.
- (7) Wei, X.; Li, S.; Wang, W.; Zhang, X.; Zhou, W.; Xie, S.; Liu, H. Recent advances in structure separation of single-wall carbon nanotubes and their application in optics, electronics, and optoelectronics. *Adv. Sci.* **2022**, *9*, 2200054.
- (8) Yang, F.; Wang, M.; Zhang, D.; Yang, J.; Zheng, M.; Li, Y. Chirality pure carbon nanotubes: growth, sorting, and characterization. *Chem. Rev.* **2020**, *120*, 2693–2758.
- (9) Guo, X. Single-molecule electrical biosensors based on single-walled carbon nanotubes. *Adv. Mater.* **2013**, *25*, 3397–3408.
- (10) Wang, F.; Matsuda, K.; Rahman, A. M.; Peng, X.; Kimura, T.; Komatsu, N. Simultaneous discrimination of handedness and diameter of single-walled carbon nanotubes (SWNTs) with chiral diporphyrin nanotweezers leading to enrichment of a single enantiomer of (6,S)-SWNTs. *J. Am. Chem. Soc.* **2010**, *132*, 10876–10881.
- (11) Akazaki, K.; Toshimitsu, F.; Ozawa, H.; Fujigaya, T.; Nakashima, N. Recognition and one-pot extraction of right- and left-handed semiconducting single-walled carbon nanotube enantiomers using fluorene-binaphthol chiral copolymers. *J. Am. Chem. Soc.* **2012**, *134*, 12700–12707.
- (12) Ishimaru, W.; Kim, C.; Toshimitsu, F.; Staykov, A.; Nakashima, N. One-pot separation of semiconducting single-walled carbon

nanotubes and their enantiomer recognition based on self-organized supramolecular riboflavin (vitamin B2) motifs. *J. Phys. Chem. C* **2022**, *126*, 9909–9917.

(13) Green, A. A.; Duch, M. C.; Hersam, M. C. Isolation of single-walled carbon nanotube enantiomers by density differentiation. *Nano Res.* **2009**, *2*, 69–77.

(14) Ghosh, S.; Bachilo, S. M.; Weisman, R. B. Advanced sorting of single-walled carbon nanotubes by nonlinear density-gradient ultracentrifugation. *Nat. Nanotechnol.* **2010**, *5*, 443–450.

(15) Ao, G.; Streit, J. K.; Fagan, J. A.; Zheng, M. Differentiating left- and right-handed carbon nanotubes by DNA. *J. Am. Chem. Soc.* **2016**, *138*, 16677–16685.

(16) Li, H.; Gordeev, G.; Garrity, O.; Peyyety, N. A.; Selvasundaram, P. B.; Dehm, S.; Krupke, R.; Cambre, S.; Wenseleers, W.; Reich, S.; et al. Separation of specific single-enantiomer single-wall carbon nanotubes in the large-diameter regime. *ACS Nano* **2020**, *14*, 948–963.

(17) Liu, H.; Tanaka, T.; Kataura, H. Optical isomer separation of single-chirality carbon nanotubes using gel column chromatography. *Nano Lett.* **2014**, *14*, 6237–6243.

(18) Tanaka, T.; Urabe, Y.; Hirakawa, T.; Kataura, H. Simultaneous chirality and enantiomer separation of metallic single-wall carbon nanotubes by gel column chromatography. *Anal. Chem.* **2015**, *87*, 9467–9472.

(19) Wei, X.; Tanaka, T.; Yomogida, Y.; Sato, N.; Saito, R.; Kataura, H. Experimental determination of excitonic band structures of single-walled carbon nanotubes using circular dichroism spectra. *Nat. Commun.* **2016**, *7*, 12899.

(20) Wei, X.; Tanaka, T.; Hirakawa, T.; Yomogida, Y.; Kataura, H. Determination of enantiomeric purity of single-wall carbon nanotubes using flavin mononucleotide. *J. Am. Chem. Soc.* **2017**, *139*, 16068–16071.

(21) Xu, L.; Valásek, M.; Hennrich, F.; Sedghamiz, E.; Penalzoza-Amion, M.; Häussinger, D.; Wenzel, W.; Kappes, M. M.; Mayor, M. Enantiomeric separation of semiconducting single-walled carbon nanotubes by acid cleavable chiral polyfluorene. *ACS Nano* **2021**, *15*, 4699–4709.

(22) Wei, X.; Tanaka, T.; Hirakawa, T.; Tsuzuki, M.; Wang, G.; Yomogida, Y.; Hirano, A.; Kataura, H. High-yield and high-throughput single-chirality enantiomer separation of single-wall carbon nanotubes. *Carbon* **2018**, *132*, 1–7.

(23) Maeda, Y.; Konno, Y.; Yamada, M. Helicity sorting and optical resolution of functionalized single-walled carbon nanotubes and their optical properties. *J. Phys. Chem. C* **2020**, *124*, 21886–21894.

(24) Gu, J.; Han, J.; Liu, D.; Yu, X.; Kang, L.; Qiu, S.; Jin, H.; Li, H.; Li, Q.; Zhang, J. Solution-processable high-purity semiconducting SWCNTs for large-area fabrication of high-performance thin-film transistors. *Small* **2016**, *12*, 4993–4999.

(25) Liu, L.; Han, J.; Xu, L.; Zhou, J.; Zhao, C.; Ding, S.; Shi, H.; Xiao, M.; Ding, L.; Ma, Z.; et al. Aligned, high-density semiconducting carbon nanotube arrays for high-performance electronics. *Science* **2020**, *368*, 850–856.

(26) Wang, J.; Nguyen, T. D.; Cao, Q.; Wang, Y.; Tan, M. Y.; Chan-Park, M. B. Selective surface charge sign reversal on metallic carbon nanotubes for facile ultrahigh purity nanotube sorting. *ACS Nano* **2016**, *10*, 3222–3232.

(27) Tulevski, G. S.; Franklin, A. D.; Afzali, A. High purity isolation and quantification of semiconducting carbon nanotubes via column chromatography. *ACS Nano* **2013**, *7*, 2971–2976.

(28) Ichinose, Y.; Eda, J.; Yomogida, Y.; Liu, Z.; Yanagi, K. Extraction of high-purity single-chirality single-walled carbon nanotubes through precise pH control using carbon dioxide bubbling. *J. Phys. Chem. C* **2017**, *121*, 13391–13395.

(29) Lyu, M.; Meany, B.; Yang, J.; Li, Y.; Zheng, M. Toward complete resolution of DNA/carbon nanotube hybrids by aqueous two-phase systems. *J. Am. Chem. Soc.* **2019**, *141*, 20177–20186.

(30) Yang, X.; Liu, T.; Li, R.; Yang, X.; Lyu, M.; Fang, L.; Zhang, L.; Wang, K.; Zhu, A.; Zhang, L.; et al. Host-guest molecular interaction

enabled separation of large-diameter semiconducting single-walled carbon nanotubes. *J. Am. Chem. Soc.* **2021**, *143*, 10120–10130.

(31) Flavel, B. S.; Kappes, M. M.; Krupke, R.; Hennrich, F. Separation of single-walled carbon nanotubes by 1-dodecanol-mediated size-exclusion chromatography. *ACS Nano* **2013**, *7*, 3557–3564.

(32) Wei, L.; Flavel, B. S.; Li, W.; Krupke, R.; Chen, Y. Exploring the upper limit of single-walled carbon nanotube purity by multiple-cycle aqueous two-phase separation. *Nanoscale* **2017**, *9*, 11640–11646.

(33) Li, H.; Gordeev, G.; Garrity, O.; Reich, S.; Flavel, B. S. Separation of small-diameter single-walled carbon nanotubes in one to three steps with aqueous two-phase extraction. *ACS Nano* **2019**, *13*, 2567–2578.

(34) Liang, L.; Xie, W.; Fang, S.; He, F.; Yin, B.; Tlili, C.; Wang, D.; Qiu, S.; Li, Q. High-efficiency dispersion and sorting of single-walled carbon nanotubes via non-covalent interactions. *J. Mater. Chem. C* **2017**, *5*, 11339–11368.

(35) Zheng, M.; Semke, E. D. Enrichment of single chirality carbon nanotubes. *J. Am. Chem. Soc.* **2007**, *129*, 6084–6085.

(36) Khripin, C. Y.; Tu, X.; Heddlston, J. M.; Silvera-Batista, C.; Hight Walker, A. R.; Fagan, J.; Zheng, M. High-resolution length fractionation of surfactant-dispersed carbon nanotubes. *Anal. Chem.* **2013**, *85*, 1382–1388.

(37) Miyata, Y.; Shiozawa, K.; Asada, Y.; Ohno, Y.; Kitaura, R.; Mizutani, T.; Shinohara, H. Length-sorted semiconducting carbon nanotubes for high-mobility thin film transistors. *Nano Res.* **2011**, *4*, 963–970.

(38) Huang, X.; Mclean, R. S.; Zheng, M. High-resolution length sorting and purification of DNA-wrapped carbon nanotubes by size-exclusion chromatography. *Anal. Chem.* **2005**, *77*, 6225–6228.

(39) Noguchi, Y.; Fijigaya, T.; Niidome, Y.; Nakashima, N. Single-walled carbon nanotubes/DNA hybrids in water are highly stable. *Chem. Phys. Lett.* **2008**, *455*, 249–251.

(40) Hennrich, F.; Li, W.; Fischer, R.; Lebedkin, S.; Krupke, R.; Kappes, M. M. Length-sorted, large-diameter, polyfluorene-wrapped semiconducting single-walled carbon nanotubes for high-density, short-channel transistors. *ACS Nano* **2016**, *10*, 1888–1895.

(41) Naumov, A. V.; Ghosh, S.; Tsybouski, D. A.; Bachilo, S. M.; Weisman, R. B. Analyzing absorption backgrounds in single-walled carbon nanotube spectra. *ACS Nano* **2011**, *5*, 1639–1648.

(42) Hirano, A.; Tanaka, T.; Urabe, Y.; Kataura, H. Purification of single-wall carbon nanotubes by controlling the adsorbability onto agarose gels using deoxycholate. *J. Phys. Chem. C* **2012**, *116*, 9816–9823.

(43) Liu, L.; Wei, X.; Yao, Z.; Li, X.; Wang, W.; Wang, Y.; Zhou, W.; Xiong, F.; Kataura, H.; Xie, S.; et al. Separation of metallic and semiconducting single-wall carbon nanotubes using sodium hydoexocholate surfactant. *J. Phys. Chem. C* **2022**, *126*, 3787–3795.

(44) Cherukuri, T. K.; Tsybouski, D. A.; Weisman, R. B. Length- and defect-dependent fluorescence efficiencies of individual single-walled carbon nanotubes. *ACS Nano* **2012**, *6*, 843–850.

(45) Heller, D. A.; Mayrhofer, R. M.; Baik, S.; Grinkova, Y. V.; Usrey, M. L.; Strano, M. S. Concomitant length and diameter separation of single-walled carbon nanotubes. *J. Am. Chem. Soc.* **2004**, *126*, 14567–14573.

(46) Fagan, J. A.; Simpson, J. R.; Bauer, B. J.; Lacerda, S. H. D. P.; Becker, M. L.; Chun, J.; Migler, K. B.; Walker, A. R. H.; Hobbie, E. K. Length-dependent optical effects in single-wall carbon nanotubes. *J. Am. Chem. Soc.* **2007**, *129*, 10607–10612.

(47) Naumov, A. V.; Tsybouski, D. A.; Bachilo, S. M.; Weisman, R. B. Length-dependent optical properties of single-walled carbon nanotube samples. *Chem. Phys.* **2013**, *422*, 255–263.

(48) Chiu, K.-C.; Falk, A. L.; Ho, P.-H.; Farmer, D. B.; Tulevski, G.; Lee, Y.-H.; Avouris, P.; Han, S.-J. Strong and broadly tunable plasmon resonances in thick films of aligned carbon nanotubes. *Nano Lett.* **2017**, *17*, 5641–5645.

(49) Morimoto, T.; Joung, S.-K.; Saito, T.; Futaba, D. N.; Hata, K.; Okazaki, T. Length-dependent plasmon resonance in single-walled carbon nanotubes. *ACS Nano* **2014**, *8*, 9897–9904.

(50) Li, H.; Smis, C. M.; Kang, R.; Biedermann, F.; Fagan, J. A.; Flavel, B. S. Isolation of the (6,5) single-wall carbon nanotube enantiomers by surfactant-assisted aqueous two-phase extraction. *Carbon* **2023**, *204*, 475–483.

(51) Wei, X.; Tanaka, T.; Akizuki, N.; Miyauchi, Y.; Matsuda, K.; Ohfuchi, M.; Kataura, H. Single-chirality separation and optical properties of (5,4) single-wall carbon nanotubes. *J. Phys. Chem. C* **2016**, *120*, 10705–10710.

(52) Sebastian, F. L.; Zorn, N. F.; Settele, S.; Lindenthal, S.; Berger, F. J.; Bendel, C.; Li, H.; Flavel, B. S.; Zaumseil, J. Absolute quantification of sp^3 defects in semiconducting single-wall carbon nanotubes by Raman spectroscopy. *J. Phys. Chem. Lett.* **2022**, *13*, 3542–3548.

(53) Li, S.; Wei, X.; Li, L.; Cui, J.; Yang, D.; Wang, Y.; Zhou, W.; Xie, S.; Hirano, A.; Tanaka, T.; et al. Quantitative analysis of the effect of reabsorption on the Raman spectroscopy of distinct (n, m) carbon nanotubes. *Anal. Methods* **2020**, *12*, 2376–2384.

(54) Yomogida, Y.; Tanaka, T.; Tsuzuki, M.; Wei, X.; Kataura, H. Automatic sorting of single-chirality single-wall carbon nanotubes using hydrophobic cholates: implications for multicolor near-infrared optical technologies. *ACS Appl. Nano Mater.* **2020**, *3*, 11289–11297.